PCCP

Accepted Manuscript

ROYAL SOCIETY OF CHEMISTRY

www.rsc.org/pccp

submitted to Phys. Chem. Chem. Phys.

Mechanisms and Energetics for N-Glycosidic Bond Cleavage of Protonated 2'-Deoxyguanosine and Guanosine

R. R. Wu, Yu Chen, and M. T. Rodgers*

Department of Chemistry, Wayne State University, Detroit, Michigan 48202, United States

Abstract

Experimental and theoretical investigations suggest that hydrolysis of N-glycosidic bonds generally involves a concerted S_N2 or a stepwise S_N1 mechanism. While theoretical investigations have provided estimates for the intrinsic activation energies associated with N-glycosidic bond cleavage reactions, experimental measurements to validate the theoretical studies remain elusive. Here we report experimental investigations for N-glycosidic bond cleavage of the protonated guanine nucleosides, $[dGuo+H]^+$ and $[Guo+H]^+$, using threshold collision-induced dissociation (TCID) techniques. Two major dissociation pathways involving N-glycosidic bond cleavage, resulting in production of protonated guanine or the elimination of neutral guanine are observed in competition for both $[dGuo+H]^+$ and $[Guo+H]^+$. The detailed mechanistic pathways for the N-glycosidic bond cleavage reactions observed are mapped via electronic structure calculations. Excellent agreement between the measured and B3LYP calculated activation energies and reaction enthalpies for N-glycosidic bond cleavage of $[dGuo+H]^+$ and $[Guo+H]^+$ in the gas phase is found indicating that these dissociation pathways involve stepwise E1 mechanisms in analogy to the S_N1 mechanisms that occur in the condensed phase. In contrast, MP2 is found to significantly overestimate the activation energies and slightly overestimate the reaction enthalpies. The 2'-hydroxyl substituent is found to stabilize the N-glycosidic bond such that $[Guo+H]^+$ requires ~25 kJ/mol more than $[dGuo+H]^+$ to activate the glycosidic bond.

Keywords: activation energies, 2'-deoxyguanosine, guanosine, protonation, N-glycosidic bond cleavage, dissociation mechanisms.

Introduction

Guanine, one of the two purine bases that occurs in both DNA and RNA nucleic acids, which when linked to 2'-deoxyribose or ribose via an N-glycosidic bond, forms 2'-deoxyguanosine (dGuo) or guanosine (Guo), respectively. The chemical structures of dGuo and Guo are shown in Figure 1. Among the canonical DNA and RNA nucleobases, with 78 electrons, guanine is the largest, has the most complex electronic structure, and exhibits the lowest oxidation potential and ionization energy.[1,2] As a result, guanine residues are susceptible to oxidative damage involving alkylating and oxidizing agents,[3,4] halogens,[5] and phenoxyl and aromatic radicals.[6] The most commonly observed form of oxidatively damaged guanine is 8-oxoguanine.[7] Transformation of DNA from the B form to the Z form can be promoted by certain substitutions at the C8 position.[8,9] The C8 position has also been found to be the preferred binding site for certain carcinogens.[10] In RNA, there are more than 20 natural variants of guanine.2 The N7 and O6 positions of guanine have been found to preferentially interact with transition metal cations.[11,12] Moreover, among the nucleobases, guanine has the special ability to form self-assembled tetrameric species (G-quartets) because guanine possesses two hydrogen bond donor (N1–H and N2–H) as well as two hydrogen bond acceptor (O6 and N7) moieties. When G-quartets stack on top of one another, they form a G-quadruplex.[13,14] Studies of the structure of G-quadruplexes have attracted a great deal of attention because of the many G-rich, biologically significant, genome regions including the immunoglobulin switch regions,[15] gene promoter regions,[16] interrupted sequences associated with human diseases,[17] and the end of chromosomes (telomeres).[18] Because of these interesting characteristics of guanine, extensive experimental [19 – 39] and theoretical[39– 48] studies have been performed on guanine, guanine derivatives, and the DNA and RNA guanine nucleosides: dGuo and Guo.

The N-glycosidic bond,[49] connecting the nucleobase to the 2'-deoxyribose or ribose moieties, maintains the integrity of the overall structures of nucleic acids and is ultimately crucial in preserving the biological and genetic information that nucleic acids carry. For this reason, N-glycosidic bonds are extremely stable under normal biological conditions. Cleavage

of the N-glycosidic bond is of great importance because the nucleobases are susceptible to modifications and damage, and the removal of undesirable nucleobases must necessarily involve cleavage of this bond.[50] Therefore, glycosidic bond cleavage reactions are commonly involved in nucleobase salvage[51–53] and base excision repair pathways,[54,55] which are catalyzed by various enzymes.[50,56,57] Glycosidic bond cleavage reactions have been extensively investigated both experimentally[58–68] and theoretically.[69–73] These studies suggest that under biological conditions, two dissociative mechanisms, a concerted S_N2 and a stepwise S_N1, are usually involved in glycosidic bond cleavage processes. These two mechanisms are difficult to distinguish and may even accompany one another.[56,64,74] The stepwise S_N1 mechanism, involving the departure of the nucleobase (D_N) and the addition of the nucleophile (A_N), is found to be more prevalent for enzymatic glycosidic bond cleavage such that the active-site residues of the catalyst enable nucleobase departure (D_N) via hydrogen-bonding interactions or protonation of the base,[75–77] and the activated nucleophiles attack the sugar after the removal of the base.[78,79] Acidic conditions or alkylating agents generally accelerate glycosidic bond hydrolysis,[80,81] as protonation makes the nucleobase a better leaving group, lowers the barrier to activated dissociation, and facilitates cleavage of the glycosidic bond.[68]

The canonical DNA and RNA nucleosides, as the smallest and simplest building blocks of nucleic acids that contain an N-glycosidic bond, serve as good models for studies of the intrinsic mechanism and energetics for N-glycosidic bond cleavage. Rios-Font et al.[69] explored the potential energy surfaces (PESs) for non-enzymatic glycosidic bond hydrolysis of neutral and protonated 3'-O-methyl-2'-deoxyguanosine (dGuom[3], where protection via 3'-O-methylation was used to avoid spurious hydrogen bonds) using quantum chemical calculations to discuss the influence of protonation on the mechanism of glycosidic bond hydrolysis. They proposed a stepwise S_N1 mechanism and found that N7 protonation strongly catalyzes the hydrolysis of the glycosidic bond, making guanine a better leaving group.

Glycosidic bond cleavage reactions commonly involve protonation of the departing nucleobase by an acid, thereby assisting nucleophilic attack and lowering the associated

activation barrier.[76] However, the intrinsic effect of protonation on the N-glycosidic bond dissociation mechanisms and the associated quantitative thermochemistry remain elusive. Therefore, in this work, we elucidate the detailed mechanisms for N-glycosidic bond cleavage of $[dGuo+H]^+$ and $[Guo+H]^+$ and quantitatively determine the activations energies (AEs) and reaction enthalpies (ΔH_{rxn}s) for these systems. N-glycosidic bond cleavage of the protonated guanine nucleosides, $[dGuo+H]^+$ and $[Guo+H]^+$, in the gas phase are examined using both guided ion beam tandem mass spectrometry techniques, via measurement and thermochemical analysis of the energy-dependent collision-induced dissociation (CID) cross sections, and theoretical electronic structure calculations by explicitly mapping the PESs for the N-glycosidic bond cleavage reactions observed for $[dGuo+H]^+$ and $[Guo+H]^+$.

In complementary work published previously, we examined the structures of the protonated forms of the canonical DNA and RNA nucleosides using synergistic infrared multiple photon dissociation (IRMPD) action spectroscopy techniques and electronic structure calculations to determine the most favorable site of protonation and the stable low-energy structures populated experimentally.[39,82–85] In particular, key findings of the IRMPD study of $[dGuo+H]^+$ and $[Guo+H]^+$[39] confirm that N7 is the most favorable protonation site. The O6 and N3 protonated conformers lie more than 35 kJ/mol higher in energy than the N7 protonated ground-state conformers. These ground-state conformers are assumed to be the structures accessed in the CID experiments performed here as the same ionization technique, electrospray ionization (ESI) was used in the IRMPD study and in the present work, such that the N-7 protonated ground-state conformers are used as the initial structures along the PESs for the N-glycosidic bond cleavage reactions of these protonated guanine nucleosides. The theoretical electronic structure calculations provide important molecular parameters for experimental-threshold analyses, and detailed information of the PESs for glycosidic bond cleavage. The TCID techniques provide accurate quantitative determination of the AEs and ΔH_{rxn}s for N-glycosidic bond cleavage. The B3LYP/6-311+G(2d,2p) and MP2(full)/6-311+G(2d,2p) levels of theory were employed to determine the relative energies along the PESs and to provide

theoretical estimates for the measured threshold energies. Comparison of theoretical and experimental results also enables the ability of these two levels of theory for describing the mechanism and energetics for N-glycosidic bond cleavage to be evaluated. Comparison of the mechanisms and energetics for glycosidic bond cleavage of $[dGuo+H]^+$ and $[Guo+H]^+$ enables the effect of the 2'-hydroxyl substituent on the dissociation mechanisms and stability of the N-glycosidic bond to be determined. Because cleavage of the N-glycosidic bond is an important biological process that occurs with great frequency in nature, the accurate quantitative thermochemical information for N-glycosidic bond cleavage extracted from this work lays the foundation for future glycosidic bond cleavage studies of the other protonated canonical as well as modified DNA and RNA nucleosides. Combined these studies will enable the effects of the identity of the nucleobase and modifications on the mechanisms and energetics for N-glycosidic bond cleavage to be more thoroughly understood. Moreover, previous investigations of the dissociation mechanisms of dinucleotides and RNA phosphodiester backbones in the gas-phase using mass spectrometry (MS) based approaches have shown the importance of understanding the intrinsic dissociative behavior of nucleic acid constituents in the absence of solvent.[58,59,86] Therefore, the knowledge gained from the studies of the mechanisms for glycosidic bond cleavage in the gas phase can be further correlated and applied to physiologically relevant glycosidic bond cleavage processes.

Methods

General Experimental Procedures. Cross sections for collision-induced dissociation (CID) of $[dGuo+H]^+$ and $[Guo+H]^+$ were measured using a custom built guided ion beam tandem mass spectrometer (GIBMS). The original design of our GIBMS instrument has previously been described in detail,[87] but has been modified to couple it to an ESI source.[88,89] The protonated nucleosides are generated by ESI from solutions containing 0.1 mM of the nucleoside, dGuo or Guo, and 1mM hydrochloric acid (HCl) in a mixture of 50%:50% MeOH/H_2O. Droplets emanating from the 35 gauge SS ESI needle are introduced into the vacuum region through

capillary tubing, biased at 20–50 V, and heated to 100–120 °C. The ions are focused and thermalized in an rf ion funnel[90,91] and hexapole ion guide collision cell interface. The thermalized ions are extracted from the hexapole ion guide, and accelerated and focused into a magnetic sector momentum analyzer for selection of the reactant protonated nucleoside. The mass-selected ions are decelerated to a desired kinetic energy by an exponential retarder and focused into an octopole ion guide that traps the ions in the radial direction,[92] thereby providing an ideal environment for efficient collection of species scattered in the collision-induced dissociation event. The octopole passes through a static gas cell containing xenon at low pressure (0.05–0.20 mTorr) to ensure that multiple ion-neutral collisions are improbable. Reasons for choosing xenon as the preferred collision gas have been described elsewhere.[93–95] Product ions and undissociated protonated nucleosides drift to the end of the octopole where they are guided and focused into a quadrupole mass filter for the second stage of mass analysis. The ions are detected using a secondary electron scintillation detector of the Daly type and standard pulse counting techniques.[96]

Data Handling. Measured reactant and product ion intensities are converted to absolute CID cross sections as described previously using a Beer's law analysis.[97] The laboratory ion kinetic energies are converted to energies in the center-of-mass frame, E_{CM}, which corresponds to the energy available to the dissociation process, using the formula, $E_{CM} = E_{lab}\, m/(m+M)$, where M and m are the masses of the protonated nucleoside, $[dGuo+H]^+$ or $[Guo+H]^+$, and neutral Xe reactants, respectively. The absolute zero and distribution of the laboratory ion kinetic energies are determined using the octopole ion guide as a retarding potential analyzer as previously described.[97] Pressure-dependent studies of all CID cross sections are performed and results extrapolated to zero pressure of the Xe reactant to provide results corresponding to rigorously single collision conditions, and data that can be analyzed to provide reliable thermochemistry.[98] Additional details regarding the data handling procedures can be found in the Electronic Supplementary Information.

Theoretical Calculations. The Gaussian 09 suite of programs[99] was used to map the detailed mechanisms and provide theoretical estimates of the energetics for the N-glycosidic bond cleavage reactions of $[dGuo+H]^+$ and $[Guo+H]^+$. The most stable structures of $[dGuo+H]^+$ and $[Guo+H]^+$ determined in the IRMPD spectroscopy study[39] were used as reactant structures for the relaxed potential energy scans. The scans were performed at the B3LYP/6-31G(d) level of theory and facilitate generation of good initial guesses for the transition state (TS) structures. Transition state calculations (TS, QST2 and QST3)[100,101] performed at B3LYP/6-311+G(d,p) level of theory enable localization of the optimized TS. Intrinsic reaction coordinate (IRC) calculations also performed at the B3LYP/6-311+G(d,p) level of theory are used to confirm that the optimized TS structures properly connect reactants and the various intermediates (Ints) or products along the N-glycosidic bond dissociation pathways. Vibrational analyses of the geometry-optimized structures were performed at the B3LYP/6-311+G(d,p) level of theory to determine the vibrational frequencies for use in modeling of the CID data. The calculated frequencies were scaled by a factor of 0.99.[102] The scaled vibrational frequencies and rotational constants are listed in Tables S1 and S2 of the Electronic Supplementary Information. Single point energy calculations were performed at the B3LYP/6-311+G(2d,2p) and MP2(full)/6-311+G(2d,2p) levels of theory for all species (reactants, TSs, Ints, and products) relevant to the N-glycosidic bond cleavage pathways observed experimentally. To obtain accurate energetics, zero point energy (ZPE) corrections are included for all structures, and basis set superposition error (BSSE) corrections[103,104] are also included for the CID products.

Thermochemical Analysis. The threshold regions of the measured CID cross sections for N-glycosidic bond cleavage of $[dGuo+H]^+$ and $[Guo+H]^+$ resulting in elimination of the protonated nucleobase, $[Gua+H]^+$ or loss of neutral nucleobase, Gua, are first modeled independently using the empirical threshold law of eq 1,

$$\sigma(E) = \sigma_0 \sum_i g_i (E + E_i - E_0)^n / E \qquad (1)$$

Analyses of the total CID cross sections using eq 1 are also performed as these results can be more reliable when the lowest energy pathway is significantly affected by competition with another dissociation channel. Upon N-glycosidic bond cleavage, the nucleobase and sugar moieties compete for the excess proton. In order to properly analyze competitive effects in the dissociation process and extract accurate threshold energies from these experimental CID cross sections, the statistical model of eq 1 is modified to incorporate competition between the two major N-glycosidic bond cleavage pathways as shown in eq 2 and described in detail previously.[105–107]

$$\sigma_j = (E) = \frac{n\sigma_{0,j}}{E}\sum_i g_i \int_0^{E+E_i-E_0} \frac{k_j(E^*)}{k_{tot}(E^*)}[1-e^{-k_{tot}(E^*)\tau}](\Delta E)^{n-1}d(\Delta E) \quad (2)$$

The results of competitive analyses using eq 2 are compared with those for independent modeling of the two primary and the total product cross sections with eq 1 to assess the effects of competition on the threshold energies. In particular, the density of ro-vibrational states, *i*, is determined using Beyer-Swinehart algorithm.[108–110] Details of eqs 1 and 2 are described in the Electronic Supplementary Information.

For simple CID processes corresponding to noncovalent bond cleavage reactions, the TSs are loose and product-like such that the TS vibrations used are the frequencies corresponding to the final products. The transitional frequencies, those that become rotations and translations of the completely dissociated products, are treated as rotors corresponding to a phase space limit (PSL) model as described in detail elsewhere.[106] In this work, the N-glycosidic bond cleavage reactions observed are activated dissociation processes, such that the protonated nucleoside must pass over TTSs to produce the observed dissociation products. Previous studies have verified the efficacy in modeling CID reactions that compete through loose as well as loose vs tight TSs.[111–119] Competitive analysis of the thresholds for the two primary CID pathways involving N-glycosidic bond cleavage are performed making differing assumptions about the TSs that control the rates of dissociation.[107] In all cases, glycosidic bond cleavage leading to elimination

of $[Gua+H]^+$ is modeled using a TTS model, associated with either the first or second TS along the PES for this dissociation pathway, TS_1 or TS_2, as these TSs lie above the product asymptote. However, the TTS along the pathway for glycosidic bond cleavage leading to loss of neutral Gua, TS_n, lies below the product asymptote and thus the data is modeled in three ways, using TS_n, a PSL TS, and a TS_n/PSL switching (SW) TS. Results of these analyses are compared with theoretical predications to establish the most appropriate way to analyze and interpret the thresholds for glycosidic bond cleavage of $[dGuo+H]^+$ and $[Guo+H]^+$. Overall, this leads to six distinct models being examined to describe the competitive dissociation of each of the protonated nucleosides. Additional details of the thermochemical analysis for the glycosidic bond cleavages can be found in the Electronic Supplementary Information.

Results

Cross Sections for Collision-Induced Dissociation. Experimental cross sections for collision-induced dissociation (CID) of $[dGuo+H]^+$ and $[Guo+H]^+$ with Xe were measured as a function of collision energy and are shown in Figure 2. For both protonated nucleosides, $[Nuo+H]^+ = [dGuo+H]^+$ and $[Guo+H]^+$, the primary and the lowest energy dissociation pathway corresponds to N-glycosidic bond cleavage resulting in endothermic loss of the protonated nucleobase, $[Gua+H]^+$, in the CID reactions represented by eq 3.

$$[Nuo+H]^+ + Xe \rightarrow [Gua+H]^+ + [Nuo\text{-}Gua] + Xe \quad (3)$$

In both cases, glycosidic bond cleavage resulting in loss of the neutral nucleobase, Gua, is observed in competition with elimination of the protonated nucleobase, $[Gua+H]^+$, as the next most favorable dissociation pathway, in the CID reactions represented by eq 4.

$$[Nuo+H]^+ + Xe \rightarrow [Nuo\text{-}Gua+H]^+ + Gua + Xe \quad (4)$$

Thus, the excess proton can be competitively retained either on the nucleobase or the sugar moieties, suggesting that an important transition state or intermediate along the dissociation coordinate is that of a proton-bound complex of the nucleobase and sugar moieties. As can be seen in Figure 2, the apparent thresholds for N-glycosidic bond cleavage shift to higher energies

from $[dGuo+H]^+$ to $[Guo+H]^+$, suggesting that the 2'-hydroxyl substituent stabilizes the glycosidic bond.

At elevated energies, sequential fragmentation of the protonated sugar moieties of eq 4 is also observed. The mass-to-charge ratio (*m/z*) and proposed chemical composition of each sequential ionic product (shown using smaller red symbols in Figure 2) are listed in Table S3. We are not particularly interested in the sequential fragmentation of the sugar moieties, and thus these pathways will not be examined or discussed further. However, to facilitate accurate threshold analysis, when analyzing the pathway leading to the elimination of neutral Gua (eq 4), the cross sections of the sequential fragment ions are added to the cross section for loss of the neutral nucleobase to properly describe the energy dependence for this pathway in the absence of sequential dissociation.

Theoretical Results. The ground-state structures of $[dGuo+H]^+$ and $[Guo+H]^+$ were previously reported; detailed descriptions can be found in our previous IRMPD study.[39] Both ground-state structures are shown in Figure 1. As can be seen in the figure, N7 is predicted as the most favorable site of protonation. Both $[dGuo+H]^+$ and $[Guo+H]^+$ exhibit highly parallel conformations, suggesting that the 2'-hydroxyl substituent does not exert a significant influence on the conformational features of the ground-state conformations of these species. The intramolecular hydrogen-bonding interaction between the 2'- and 3'-hydroxyl substituents of $[Guo+H]^+$ induces a slight change in the orientation of the 3'-hydroxyl substituent as compared to when this interaction is absent, as in $[dGuo+H]^+$. The presence of the 2'-hydroxyl substituent does lead to a slight contraction of the glycosidic bond C1'–N9, which is 1.508 Å long in $[dGuo+H]^+$ and decreases to 1.498 Å in $[Guo+H]^+$. This change also suggests that the 2'-hydroxyl substituent increases the stability of the glycosidic bond, consistent with the apparent CID thresholds for reactions 3 of $[dGuo+H]^+$ and $[Guo+H]^+$. The most stable O6 and N3 protonated conformers lie much higher in energy than the N7 protonated ground-state conformers of $[dGuo+H]^+$ and $[Guo+H]^+$ and are shown in Figure S1. A more comprehensive

discussion of the N7, O6, and N3 protonated low-energy conformers of $[dGuo+H]^+$ and $[Guo+H]^+$ is given in the IRMPD study of these systems.[39]

N-Glycosidic Bond Cleavage of $[dGuo+H]^+$ and $[Guo+H]^+$ Complexes. To allow appropriate thermochemical analysis of the two primary activated dissociation pathways, PESs for N-glycosidic bond cleavage of $[dGuo+H]^+$ and $[Guo+H]^+$ are mapped out. Relative energetics calculated using both the B3LYP and MP2 levels of theory for all species involved in these two activated dissociation pathways are listed in Table 1. In particular, the relative energies of the reactant and the rate-determining TSs are determined as theoretical estimates for the AEs, whereas the relative energies of the reactants and CID products (including BSSE corrections) are determined as theoretical estimates for the ΔH_{rxn}s.

The calculated PESs for N-glycosidic bond cleavage of $[Nuo+H]^+$ to produce $[Gua+H]^+$ and $[Nuo-Gua+H]^+$, and the corresponding neutral products are shown in Figure 3 and 4 for $[dGuo+H]^+$ and $[Guo+H]^+$, respectively. As shown in Figure 3a, production of $[Gua+H]^+$ from $[dGuo+H]^+$ occurs via a stepwise process. In the ground-state conformer of $[dGuo+H]^+$, the C1'–N9 glycosidic bond is 1.508 Å long (C1'–C2' = 1.530 Å, C1'–O1' = 1.396 Å, and O1'–C4' = 1.452 Å). As the glycosidic bond elongates, the N7 protonated guanine moiety gradually leaves the sugar and approaches H2', leading to TS_1, where C1'–N9 = 3.562 Å and H2'–N9 = 2.104 Å. The relative energy difference between $[dGuo+H]^+$ and TS_1 determines the first activation barrier. Using H2' as a pivot, the nucleobase rotates to form a noncanonical hydrogen-bonding interaction between N3 and H1', stabilizing the structure and leading to a stable oxacarbenium-type charged sugar intermediate, Int_1 (C1'–C2' = 1.466 Å, C1'–O1' = 1.264 Å, and O1'–C4' = 1.515 Å). Further rotation of the nucleobase to better align N9 with H2' of the charged sugar moiety facilitates proton transfer from C2' to N9, and leads to the formation of TS_2. The relative energy difference between $[dGuo+H]^+$ and TS_2 determines the height of the second activation barrier. As H2' transfers to N9 forming protonated guanine, a double bond forms between C1' and C2', (C1'=C2' = 1.341 Å), resulting in a planar neutral sugar moiety. The N7 protonated guanine and the neutral planar sugar moieties are stabilized by N9H···C2' and C8H···O5'

noncanonical hydrogen-bonding interactions, forming the final stable intermediate, Int_2. Lengthening of these noncovalent interactions, leads to smooth dissociation to the final products, protonated guanine, $[Gua+H]^+$, and the neutral 2'-deoxyribose sugar moiety, [dGuo-Gua]. B3LYP predicts that TS_1 lies 0.8 kJ/mol higher in energy than TS_2. In contrast, MP2 predicts that TS_1 is 10.9 kJ/mol lower in energy than TS_2. Both levels of theory predict that these two activation barriers exceed the final reaction enthalpy. Therefore, either TS_1 or TS_2 could be the rate-limiting TS for this dissociation pathway. Shown in Figure 3b is the calculated PES for N-glycosidic bond cleavage resulting in elimination of neutral Gua from $[dGuo+H]^+$. As can be seen in the figure, the glycosidic bond gradually elongates to 2.950 Å and a noncanonical hydrogen-bonding interaction is formed between N3 and H2' in TS_n. Although TS_n exhibits similar energetics to TS_1, the orientation and the relative position of the nucleobase to the sugar differ markedly. As the nucleobase departs from the sugar, the noncanonical N3···H2' hydrogen-bonding interaction is broken and the nucleobase reorients to form a noncanonical hydrogen-bonding interaction between N9 and H1', leading to a stable oxacarbenium-ion intermediate, Int_n (C1'–C2' = 1.469 Å, C1'–O1' = 1.260 Å, and O1'–C4' = 1.517 Å). Lengthening of the C1'–H···N9 noncovalent interaction leads to smooth dissociation into the products, a positively charged nonplanar 2'-deoxyribose moiety, [dGuo-Gua], and a noncanonical tautomer of neutral guanine, Gua. The dissociation asymptote should be the rate-limiting step for this dissociation pathway as it is calculated to lie more than 50 kJ/mol higher in energy than TS_n.

The calculated PESs for producing $[Gua+H]^+$ and $[Guo-Gua+H]^+$ from $[Guo+H]^+$ are shown in Figure 4. The dissociation mechanisms are very parallel to those for $[dGuo+H]^+$. Both levels of theory find TS_2 to be the rate-limiting step for N-glycosidic bond cleavage to produce $[Gua+H]^+$. However, TS_1 and TS_2 are found to be quite close in energy. The dissociation products are again rate-limiting for producing $[Guo-Gua+H]^+$ as they lie more than 90 kJ/mol above TS_n.

In summary, the proposed mechanisms for dissociation of $[dGuo+H]^+$ and $[Guo+H]^+$ via N-glycosidic bond cleavage resulting in loss of protonated nucleobase, $[Gua+H]^+$, involves two

major steps: 1) lengthening/cleavage of the N-glycosidic bond such that the nucleobase gradually leaves an oxacarbenium-ion like sugar moiety; and 2) transfer of the C2'-H proton from the sugar to the nucleobase. In contrast, N-glycosidic bond cleavage resulting in loss of the neutral nucleobase simply involves cleavage of the glycosidic bond with no barriers in excess of the endothermicity of dissociation. Comparison between Figures 3 and 4 indicates that the 2'-hydroxyl substituent stabilizes the glycosidic bond. Both B3LYP and MP2 theory suggest that > 20 kJ/mol more energy is required to activate the glycosidic bond of $[Guo+H]^+$ than $[dGuo+H]^+$ along either dissociation pathway.

Threshold Analysis. The model of eq 1 was used to analyze the thresholds for reactions 3 and 4 independently. The model of eq 1 was also used to analyze the thresholds for the total CID cross section (the sum of the CID cross sections of all dissociation products) of $[dGuo+H]^+$ and $[Guo+H]^+$, respectively. The data were analyzed in a variety of ways to examine the influence of the treatment of the rate-limiting TS on the threshold energies determined. Results are listed in Table S4 for $[dGuo+H]^+$ and Table S5 for $[Guo+H]^+$. According to the calculated PESs for the primary CID reactions 3, the activation energy barriers associated with TS_1 and TS_2 exceed the final reaction enthalpies and the relative stabilities of TS_1 and TS_2 are fairly similar such that either of these TSs may be determining the rate of dissociation. Therefore, the thresholds for reactions 3 and the total CID cross sections of $[dGuo+H]^+$ and $[Guo+H]^+$ were analyzed independently using a TTS model, based on either TS_1 or TS_2. As can be seen in Table S4, independent threshold analyses of the $[Gua+H]^+$ product and total CID cross sections of $[dGuo+H]^+$ produce lower threshold energies and larger kinetic shifts when TS_1 is assumed to be the rate-determining TS than when TS_2 is assumed to limit the rate of dissociation. Also, $\Delta S^{\ddagger}$ of TS_1 is much smaller than that of TS_2, indicating that TS_1 is a tighter TS than TS_2. Both reasons demonstrate that TS_1 should serve as the rate-determining TS for reaction 3 of $[dGuo+H]^+$. $\Delta S^{\ddagger}$ associated with TS_1 and TS_2 of $[Guo+H]^+$ indicates very similar tightness of these two TSs. But results listed in Table S5 for independent threshold analyses of the $[Gua+H]^+$ product and total CID cross sections of $[Guo+H]^+$ yield lower threshold energies and larger kinetic shifts when

TS_2 is assumed to be the rate-determining TS than when TS_1 is assumed to limit the dissociation rate. Therefore, TS_2 is slightly tighter than TS_1 and thus is the rate-determining step for reaction 3 of $[Guo+H]^+$. These results suggest that B3LYP predicts the relative energetics of TS_1 and TS_2 for both reactions 3 more accurately than MP2. According to the calculated PESs for the CID reactions 4, the final reaction enthalpies are > 50 kJ/mol higher in energy than TS_n. Therefore, the dissociation asymptotes for reaction 4 should be rate-determining. However, the confined phase space of TS_n could also contribute to slowing down these dissociation processes. Therefore, the thresholds for reaction 4 were modeled using a TTS model, TS_n, a loose PSL TS model, corresponding to the CID products, and a SW TS model, involving both TS_n and the PSL TS models. As indicated earlier, the product cross sections for the CID fragments arising from sequential dissociation were added to the product cross sections for reaction 4 before threshold analysis. From Tables S4 and S5, it is clear that the TTS model provides much lower threshold energies for reaction 4 than the PSL and SW TS models, which give virtually the same threshold energies for reaction 4. This suggests that when TS_n is significantly below the reaction asymptote (by > 50 kJ/mol), that it no longer affects the dissociation rate. However, the SW TS model including both TS_n and PSL better reproduces the threshold region than the PSL TS model does on its own.

The model of eq 2 was used to competitively analyze the thresholds for reactions 3 and 4 of $[dGuo+H]^+$ and $[Guo+H]^+$. Various treatments for the rate-limiting TSs controlling the dissociations are examined, and the results are listed in Table S6 for $[dGuo+H]^+$ and Table S7 for $[Guo+H]^+$. All plausible combinations of the relevant TS models are examined. In all cases, reactions 3 are modeled using the TTS models associated with the computed TSs, TS_1 or TS_2, whereas reactions 4 are modeled using either TS_n, a loose PSL TS, or a SW TS model. When TTS models are used for both pathways, TS_1 and TS_n or TS_2 and TS_n, the σ_0 values for reaction 4 are improbably large, and the thresholds of reaction 3 are pushed to higher values, whereas the thresholds of reaction 4 decrease relative to the thresholds derived from the TTS + PSL combinations. When the TTS + SW TS combination is used, the *n* values derived are the same as

that found for fits to the total CID cross sections suggesting that this approach is robust. The combination of TS_1 and SW TS for $[dGuo+H]^+$ and TS_2 and SW TS for $[Guo+H]^+$ are found to be the most reliable models for competitively fitting the CID cross sections for reactions 3 and 4. The fitting parameters derived from competitive fits for these systems are summarized in Table 2. Threshold analyses using these models are shown in Figure 5. Because TS_1 and TS_n are similar in energy and simple noncovalent bond cleavage of the weak noncanonical hydrogen-bonding interactions in Int_1 and Int_n both lead to the loss of the neutral nucleobase, we also competitively fit the CID cross sections for reactions 3 and 4 using TS1 and SW TS (TS1 + PSL), respectively. The fitting parameters derived from these fits are summarized in Table S8, and are very similar to those listed in Table 2 for fits using TS_n and SW TS. Thus, there are at least two distinct, and possibly more, glycosidic bond cleavage TSs that may be associated with elimination of the neutral nucleobase as it is the product asymptote and thus PSL TS that controls the dissociation rate.

The entropy of activation, $\Delta S^{\dagger}$, is a measure of the looseness/tightness of the TS and is also a reflection of the complexity of the system. It is largely determined by the molecular parameters used to model the energized complex and the rate-limiting TS for dissociation, but also depends on the threshold energy. The $\Delta S^{\dagger}$ values for reactions 3 of $[dGuo+H]^+$ via TS_1 and $[Guo+H]^+$ via TS_2 are 25 and 38 J/mol·K at 1000 K, indicative of fairly TTSs. In contrast, the $\Delta S^{\dagger}$ values at 1000 K for reactions 4 are 99 and 101 J/mol·K, for $[dGuo+H]^+$ and $[Guo+H]^+$, respectively, indicative of the loose PSL TSs used to model the data.

Discussion

Comparison of Theory and Experiment. The measured and calculated AEs and ΔH_{rxn}s for N-glycosidic bond cleavage of $[dGuo+H]^+$ and $[Guo+H]^+$ at 0 K are summarized in Table 3. The agreement between theory and experiment is illustrated in Figure 6. From Table 3 and Figure 6, it can be seen that for both CID pathways, $[dGuo+H]^+$ requires less energy to activate and dissociate the N-glycosidic bond than $[Guo+H]^+$. Competition between the two N-

glycosidic bond cleavage pathways for $[dGuo+H]^+$ is slightly greater than for $[Guo+H]^+$ as indicated by the smaller difference in the threshold energies for the primary dissociation pathways and the relative magnitudes of the $[Gua+H]^+$ and $[Nuo-Gua+H]^+$ product cross sections (see Figure 5). Overall, B3LYP exhibits better agreement with experiment than MP2. The mean absolute deviation (MAD) between B3LYP theory and experiment for the AEs for the elimination of $[Gua+H]^+$ from $[dGuo+H]^+$ and $[Guo+H]^+$ is 3.9 ± 3.2 kJ/mol, whereas the MAD between MP2 theory and experiment is 40.7 ± 2.2 kJ/mol. This very large MAD found for the MP2 results suggests that larger basis sets may be needed to properly describe the associated transition states for MP2 theory than that needed by B3LYP theory. The MAD between B3LYP theory and experiment for the reaction enthalpies for elimination of Gua from $[dGuo+H]^+$ and $[Guo+H]^+$ is 11.8 ± 4.7 kJ/mol, whereas the MAD between MP2 theory and experiment is 8.1 ± 2.5 kJ/mol, when BSSE corrections are included. In contrast, when the BSSE corrections are not included, the MAD between B3LYP theory and experiment improves to 6.1 ± 4.5 kJ/mol, whereas the MAD between MP2 theory and experiment degrades markedly to 44.3 ± 1.2 kJ/mol. Thus, B3LYP exhibits very good agreement with experiment whether or not BSSE corrections are included, whereas BSSE corrections are critical for reliable energetics for this dissociation pathway from MP2 theory.

Thermal Corrections. The N-glycosidic bond activation energies and dissociation enthalpies determined here at 0 K are converted to 298 K enthalpies and free energies. The enthalpy and entropy corrections are calculated using standard formulas based on harmonic oscillator and rigid rotor models and the molecular parameters (vibrational frequencies and rotational constants) determined for the B3LYP/6-311+G(d,p) optimized geometries, which are given in Tables S1 and S2 of the Electronic Supplementary Information. Table S9 lists 0 and 298 K enthalpies, free energies, and enthalpic and entropic corrections for both $[dGuo+H]^+$ and $[Guo+H]^+$. Uncertainties in the enthalpic and entropic corrections are determined by ± 10% variation in all vibrational frequencies, and additionally by ±50% variation in all frequencies below 300 cm^{-1}.

The Effect of Protonation on Glycosidic Bond Stability. The measured activation energies for N-glycosidic bond cleavage of $[dGuo+H]^+$ and $[Guo+H]^+$ of 93.6 ± 2.9 kJ/mol and 114.8 ± 2.9 kJ/mol are quite low as compared to typical covalent bonds, clearly indicating the role that protonation plays in facilitating glycosidic bond cleavage. Based on the results determined here, the intrinsic stability of the N-glycosidic bond can be effectively modeled and elucidated in the absence of solvent and stabilizing counterions. Thus, the intrinsic enhancement in reactivity for various enzyme-catalyzed glycosidic bond cleavage reactions can largely be attributed to the effects of the excess proton, whereas the molecular scaffold of the enzyme likely provides minor additional stabilization of the activated complexes.

The Effect of the 2'-Hydroxyl Substituent. As can be seen in Figure 1, the 2'-hydroxyl substituent does not exert a significant influence on the structures of the stable ground-state conformations of $[dGuo+H]^+$ and $[Guo+H]^+$. The theoretically predicted mechanisms for N-glycosidic bond cleavage of $[dGuo+H]^+$ and $[Guo+H]^+$ shown in Figures 3 and 4 are also highly parallel. Based on the experimental AEs and ΔH_{rxn}s listed in Table 3, it is clear that the 2'-hydroxyl substituent increases the AE and ΔH_{rxn} of $[Guo+H]^+$ by > 20 kJ/mol, suggesting that the 2'-hydroxyl substituent increases the stability of the N-glycosidic bond of $[Guo+H]^+$ over $[dGuo+H]^+$, consistent with the contraction of the C1'–N9 bond of $[Guo+H]^+$ in the computed structures.

Competition between Glycosidic Bond Cleavage Pathways. Thermochemical analysis of the CID cross sections indicates that the thresholds for reaction 4 exceed those for reaction 3 by > 70 kJ/mol for both $[dGuo+H]^+$ and $[Guo+H]^+$. In addition, the competition remains fairly insignificant until several hundred kJ/mol above the onset for glycosidic bond cleavage. Therefore, although the elimination of neutral guanine pathways are observed in these gas phase CID measurements, and enable the intrinsic heats of reaction for these pathways to be quantitatively determined, it is clear that they cannot play an important role in condensed phase systems. This is significant as these pathways lead to the production of neutral guanine in a noncanonical tautomeric state, which would be less useful for nucleobase salvage.

Comparison to N-Glycosidic Bond Hydrolysis of Neutral and N7 Protonated dGuom^3. In earlier work, Rios-Font et al. investigated the N-glycosidic bond hydrolysis of neutral and N7 protonated dGuom^3 via quantum chemical calculations at the B3LYP/6-31++G(d,p) level of theory.[69] For the neutral and N7 protonated species, they found that glycosidic bond hydrolysis involves different stepwise S_N1 mechanisms, leading to dihydrofurane-like and oxacarbenium ion intermediates, respectively. The S_N1 mechanisms involve the addition of H^+ from H_2O to the departing base and the addition of OH^- from H_2O to C1'. N7 protonation was found to significantly lower the activation energy, by ~110–140 kJ/mol. In the current study, in the absence of water, N-glycosidic bond cleavage occurs via a stepwise E1 mechanism. Similar to the S_N1 mechanism, the E1 processes involve D_N as the result of the glycosidic bond cleavage. The D_N step of the S_N1 process suggests that ~80 kJ/mol is required to achieve the glycosidic bond lengthening,[69] whereas that of current study suggests that ~95 kJ/mol is required to cleave the glycosidic bond in the absence of water. Thus protonation plays a more significant role in lowering the activation energy than does the presence of water. In the second step of the S_N1 process, OH^- from water, as the nucleophile, adds to C1' of the sugar moiety, while H^+ adds to the departing nucleobase. In contrast, in the second step of the E1 process presented here, the C2′ proton transfers to the departing nucleobase, and after the protonated nucleobase is produced, a double bond between C1' and C2' is formed, producing a planar sugar moiety. The similarity shared between the S_N1 and E1 processes is that, with or without water, but with the assistance of protonation, both glycosidic bond cleavage reactions go through an oxacarbenium ion intermediate of the sugar moiety. Therefore, the intrinsic effect of protonation is to facilitate the formation of this particular intermediate by yielding a much lower activation energy barrier for glycosidic bond cleavage.

Implications for Glycosidic Bond Hydrolysis in Biological Systems. The stepwise E1 mechanism for glycosidic bond cleavage of $[dGuo+H]^+$ and $[Guo+H]^+$ in the gas phase computed here and validated by threshold CID measurements strongly resembles the stepwise S_N1 mechanism for glycosidic bond hydrolysis computed for $[dGuom^3+H]^+$ in an aqueous

environment.[69] Therefore, gas-phase glycosidic bond cleavage serves as an effective model for real life glycosidic bond hydrolysis reactions that occur via a stepwise S_N1 mechanism. The activation energy for the rate-determining (glycosidic bond lengthening/cleavage) step in the absence of water is found to be ~15 kJ/mol greater than that for the glycosidic bond hydrolysis in solution. In addition, we have calculated the relative energies of all species along the PESs for producing $[Gua+H]^+$ with a polarizable continuum model (PCM) to examine the effects of solvation on this process. The results are summarized in Table 4. In comparison to Table 1, we can see that the solvent greatly stabilizes the final products; however, the relative energies of the TSs controlling the reaction rates are much less affected by the solvent. These results indicate that quantitative determinations of the activation energies for glycosidic bond cleavage in the gas phase provide reliable approximations for the AEs for glycosidic bond hydrolysis under biological conditions.

Conclusions

Results from kinetic-energy-dependent CID studies of $[dGuo+H]^+$ and $[Guo+H]^+$ with Xe find that activated dissociation leads to N-glycosidic bond cleavage producing protonated guanine and positively charged sugar moieties (and their complementary neutral losses) in competition. The thresholds for these activated dissociation pathways are interpreted to yield AEs for elimination of the protonated base, $[Gua+H]^+$, and ΔH_{rxn}s for elimination of the neutral base, Gua. N-glycosidic bond cleavage of $[Guo+H]^+$ requires more energy than $[dGuo+H]^+$, indicating that the 2'-hydroxyl substituent stabilizes the glycosidic bond although it does not significantly influence the stable low-energy conformations of $[Guo+H]^+$ vs those of $[dGuo+H]^+$. Theoretical calculations performed at the B3LYP/6-311+G(d,p) level of theory are employed to characterize the structures and mechanisms for N-glycosidic bond cleavage. Theory predicts that for both $[dGuo+H]^+$ and $[Guo+H]^+$ N-glycosidic bond cleavage resulting in loss of $[Gua+H]^+$ involves two major steps: 1) cleavage of the N-glycosidic bond and 2) proton transfer from C2' to the nucleobase. In contrast, N-glycosidic bond cleavage resulting in loss of neutral Gua,

simply involves lengthening/cleavage of the N-glycosidic bond. The TSs for "cleavage of the glycosidic bond" of these two CID channels differ somewhat: one facilitating approach of the nucleobase to align with and facilitate transfer of the C2 proton, whereas the other simply enables a smooth departure of the nucleobase. The B3LYP/6-311+G(2d,2p) and MP2(full)/6-311+G(2d,2p) levels of theory are employed to predict the relative energetics for all structures involved in the N-glycosidic bond dissociation processes. B3LYP provides excellent theoretical estimates for the AEs for the elimination of $[Gua+H]^+$, whereas MP2 theory significantly overestimates the heights of these barriers. Both B3LYP and MP2 theory provide good estimates for the ΔH_{rxn}s for elimination of Gua from $[dGuo+H]^+$ and $[Guo+H]^+$. The B3LYP values are systematically low, whereas the MP2 values are systematically high. Overall, B3LYP properly describes the energetics for glycosidic bond cleavage of $[dGuo+H]^+$ and $[Guo+H]^+$ much more effectively than MP2 theory. The relatively low measured AEs for N-glycosidic bond cleavage of $[dGuo+H]^+$ and $[Guo+H]^+$ of 93.6 ± 2.9 kJ/mol and 114.8 ± 2.9 kJ/mol clearly establish the importance of protonation in catalyzing glycosidic bond cleavage. The proposed stepwise E1 mechanism in the gas phase correlates nicely with the stepwise S_N1 mechanism under real biological conditions. In particular, the nucleobase departure (D_N) steps in both mechanisms are highly parallel and both lead to an oxacarbenium ion intermediate. The presence of water only lowers the activation energy for glycosidic bond cleavage by ~15 kJ/mol. In contrast, protonation significantly lowers the activation energy, by > 100 kJ/mol. The results determined here clearly establish that the intrinsic stability of the N-glycosidic bond can be effectively modeled and elucidated in the absence of solvent and stabilizing counterions; follow up studies of the other canonical and noncanonical DNA and RNA nucleosides will provide insight into the effects of nucleobase identity and modifications on the stability of the N-glycosidic bond.

Electronic Supplementary Information

Additional details regarding the data handling and thermochemical analysis procedures. Vibrational frequencies, average internal energies and rotational constants of the protonated nucleosides, $[dGuo+H]^+$ and $[Guo+H]^+$ as well as all species along the dissociation pathways for N-glycosidic bond cleavage. Proposed chemical compositions of the fragments of sequential dissociation of $[dGuo-Gua+H]^+$ and $[Guo-Gua+H]^+$. Fitting parameters using eqs 1 and 2 for threshold analyses for N-glycosidic bond cleavage reactions 3 and 4 of $[dGuo+H]^+$ and $[Guo+H]^+$. Enthalpies and free energies for the N-glycosidic bond cleavage of $[dGuo+H]^+$ and $[Guo+H]^+$ at 0 and 298 K. The most stable N7, O6 and N3 protonated structures of $[dGuo+H]^+$ and $[Guo+H]^+$ with their relative energetics.

Acknowledgements

This work is supported by the National Science Foundation, Grant CHE-1409420. R.R.W. also gratefully acknowledges support from a Thomas C. Rumble Graduate and Summer Dissertation Fellowships at Wayne State University. The authors also thank Wayne State University C&IT for computer time and support.

References

1 S. Bjelland and E. Seeberg, *Mutat. Res.*, 2003, **531**, 37.
2 P. A. Limbach, P. F. Crain and J. A. McCloskey, *Nucleic Acids Res.*, 1994, **22**, 2183.
3 C. J. Burrows and G. Muller, *Chem. Rev.*, 1998, **98**, 1109.
4 H. Wiseman and B. Halliwell, *Biochem. J.*, 1996, **313**, 17.
5 M. Masuda, T. Suzuki, M. D. Friesen, J. L. Ravanat, J. Cadet, B. Pignatelli, H. Nishino and H. Ohshima, *J. Biol. Chem.*, 2001, **276**, 40486.
6 J.-A. Liu, C. J. Petzold, L. E. Ramirez-Arizmendi, J. Perez and H. Kenttamaa, *J. Am. Chem. Soc.*, 2005, **127**, 12758.
7 K. C. Cheng, D. S. Cahill, H. Kasai, S. Nishimura and L. A. Loeb, *J. Biol. Chem.*, 1992, **267**, 166.
8 A. Moller, J. E. Gabriels, E. M. Lafer, A. Nordheim, A. Rich and B. D. Stollar, *J. Biol. Chem.*, 1982, **257**, 2081.
9 B. D. Stollar, E. Lafer, A. Nordheim, M. L. Pardue and A. Rich, Molecular Basis of Cancer, Part B: Macromolecular Recognition, Chemotherapy and Immunology; Rein, R., Ed.; New York: Alan R. Liss, Inc., 1985, p. 323.
10 E. Kriek, Carcinogenesis: Fundamental Mechanisms and Environmental Effects. Pullman, B., Ts'o, P. O. P., Gelboin, L. H. Eds., D. Reidel, Boston, 1980, p. 103.

11 J. V. Burda, J. Sponer and Hobza, P. *J. Phys. Chem.*, 1996, **100**, 7250.
12 B. Lippert, *Coord. Chem. Rev.*, 2000, **200**, 487–516.
13 S. Neidle and M. A. Read, *Biopolymers*, 2001, **56**, 195.
14 S. Lyonnais, C. Hounsou, M. P. Teulade-Fichou, J. Jeusset, E. L. Cam and G. Mirambeau, *Nucleic Acids Res*., 2002, **30**, 5276.
15 D. Sen, and W. Gilbert, *Nature*, 1988, **334**, 364.
16 T. Evans, E. Schon, G. Gora-Maslak, J. Patterson and A. Efstratiadis, *Nucleic Acids Res*., 1984, **12**, 8043.
17 Sarig, G., P. Weisman-Shomer, R. Erlitzki and M. Fry, *J. Biol. Chem.*, 1997, **272**, 4474.
18 E. H. Blackburn, *Cell*, 1994, **77**, 621.
19 P. F. Crain, *Mass Spectrom. Rev.*, 1990, **9**, 505.
20 M. G. Ikonomou, A. Naghipur, J. W. Lown and P. Kebarle, *Biomed. Environ. Mass Spectrom.*, 1990, **19**, 434.
21 J. M. Gregson and J. A. McCloskey, *Int. J. Mass Spectrom. Ion Processes*, 1997, **165**, 475.
22 S. Steenken and S. V. Jovanovic, *J. Am. Chem. Soc.*, 1997, **119**, 617.
23 M. Mons, I. Dimicoli, F. Piuzzi, B. Tardivel and M. Elhanine, *J. Phys. Chem. A*, 2002, **106**, 5088.
24 T. Aggerholm, S. C. Nanita, K. J. Koch and R. G. Cooks, *J. Mass. Spectrom.*, 2003, **38**, 87.
25 J. A. Hankin and R. C. Murphy, *Anal. Biochem.*, 2004, **333**, 156.
26 A. M. Kamel and B. Munson, *Eur. J. Mass Spectrom.*, 2004, **10**, 239.
27 E. Nir, I. Hünig, K. Kleinermanns and M. S. de Vries, *ChemPhysChem*, 2004, **5**, 131.
28 W. Chin, M. Mons, F. Piuzzi, B. Tardivel, I. Dimicoli, L. Gorb and J. Leszczynski, *J. Phys. Chem. A*, 2004, **108**, 8237.
29 E. S. Baker, S. L. Bernstein and M. T. Bowers, *J. Am. Soc. Mass Spectrom.*, 2005, **16**, 989.
30 R. Tuytten, F. Lemiere, W. Van Dongen, E. L. Esmans, E. Witters, W. A. Herrebout, B. J. Van Der Veken, E. Dudley and R. P. Newton, *J. Am. Soc. Mass Spectrom.*, 2005, **16**, 1291–1304.
31 R. Tuytten, F. Lemiere, E. L. Esmans, W. A. Herrebout, B. J. Van Der Veken, E. Dudley, R. P. Newton and E. Witters, *J. Am. Soc. Mass Spectrom.*, 2006, **17**, 1050.
32 E. C. M. Chen, C. Herder and E. S. Chen, *J. Mol. Struct*., 2006, **798**, 126.
33 M. Y. Choi and R. E. Miller, *J. Am. Chem. Soc.*, 2006, **128**, 7320.
34 M. Mons, F. Piuzzi, I. Dimicoli, L. Gorb and J. Leszczynski, *J. Phys. Chem. A*, 2006, **110**, 10921.
35 A. Abo-Riziq, B. O. Crews, I. Compagnon, J. Oomens, G. Meijer, G. von Helden, M. Kabeláč, P. Hobza and M. S. de Vries, *J. Phys. Chem. A*, 2007, **111**, 7529.
36 K. Seefeld, R. Brause, T. Häber and K. Kleinermanns, *J. Phys. Chem. A*, 2007, **111**, 6217.
37 H. Saigusa, S.-H. Urashima and H. Asami, *J. Phys. Chem. A*, 2009, **113**, 3455.
38 H. Asami, S. Urashima and H. Saigusa, *Phys. Chem. Chem. Phys.*, 2009, **11**, 10466.
39 R. R. Wu, B. Yang, G. Berden, J. Oomens and M. T. Rodgers, *J. Phys. Chem. B*, 2014, **118**, 14774.
40 A. K. Chandra, M. Nguyen, T. Uchimaru and T. Zeegers-Huyskens, *J. Mol. Struct.*, 2000, **555**, 61.
41 S. K. Mishra and P. C. Mishra, *J. Comput. Chem.*, 2002, **23**, 530.
42 B. Giese and D. McNaughton, *Phys. Chem. Chem. Phys.*, 2002, **4**, 5161.

43 O. V. Shishkin, O. S. Sukhanov, L. Gorb and J. Leszczynski, *Phys. Chem. Chem. Phys.*, 2002, **4**, 5359.
44 M. Hanus, F. Ryjacek, M. Kabelac, T. Kubar, T. V. Bogdan, S. A. Trygubenko and P. Hobza, *J. Am. Chem. Soc.*, 2003, **125**, 7678.
45 Y. Huang and H. Kenttamaa, *J. Phys. Chem. A*, 2004, **108**, 4485.
46 T. L. McConnell, C. A. Wheaton, K. C. Hunter and S. D. Wetmore, *J. Phys. Chem. A*, 2005, **109**, 6351.
47 R. Rios-Font, J. Bertran, L. Rodriguez-Santiago and M. Sodupe, *J. Phys. Chem. B*, 2006, **110**, 5767.
48 M. S. Ahmadi, M. Shakourian-Fard and A. Fattahi, *Struct. Chem.*, 2012, **23**, 613.
49 J. D. Watson and F. H. C. Crick, *Cold Spring Harbor Symp. Quant. Biol.*, 1953, **18**, 123.
50 J. T. Stivers and Y. L. Jiang, *Chem. Rev.*, 2003, **103**, 2729.
51 A. Bzowska, E. Kulikowska and D. Shugar, *Pharmacol. Ther.*, 2000, **88**, 349.
52 R. Pelle, V. L. Schramm and D. W. Parkin, *J. Biol. Chem.*, 1998, **273**, 2118–2126.
53 W. Versees, S. Loverix, A. Vandemeulebroucke, P. Geerlings and J. Steyaert, *J. Mol. Biol.*, 2004, **338**, 1.
54 C. D. Mol, S. S. Parikh, C. D. Putnam, T. P. Lo and J. A. Tainer, *Annu. Rev. Biophys. Biomol. Struct.*, 1999, **28**, 101.
55 C. Cao, K. Kwon, Y. L. Jiang, A. C. Drohat and J. T. Stivers, *J. Biol. Chem.*, 2003, **278**, 48012.
56 P. J. Berti and J. A. B. McCann, *Chem. Rev.*, 2006, **106**, 506.
57 V. L. Schramm, *Acc. Chem. Res.*, 2003, **36**, 588.
58 M. T. Rodgers, S. Campbell, E. M. Marzluff and J. L. Beauchamp, *Int. J. Mass Spectrom. Ion Processes*, 1994, **137**, 121.
59 M. T. Rodgers, S. Campbell, E. M. Marzluff and J. L. Beauchamp, *Int. J. Mass Spectrom. Ion Processes*, 1995, **148**, 1.
60 A. Banerjee, W. Yang, M. Karplus and G. L. Verdine, *Nature*, 2005, **434**, 612.
61 Y. Zheng, P. Cloutier, D. J. Hunting, L. Sanche and J. R. Wagner, *J. Am. Chem. Soc.*, 2005, **127**, 16592.
62 M. T. Bennett, M. T. Rodgers, A. S. Hebert, L. E. Ruslander, L. Eisele, and A. C. Drohat, *J. Am. Chem. Soc.*, 2006, **128**, 12510.
63 M. S. Bobola, S. Varadarajan, N. W. Smith, R. D. Goff, D. D. Kolstoe, A. Blank, B. Gold and J. R. Silber, *Clin. Cancer Res.*, 2007, **13**, 612.
64 J. A. B. McCann and P. J. Berti, *J. Am. Chem. Soc.*, 2007, **129**, 7055.
65 Z. Li, Y. Zheng, P. Cloutier, L. Sanche and J. R. Wagner, *J. Am. Chem. Soc.*, 2008, **130**, 5612.
66 P. Hu, S. Wang and Y. Zhang, *J. Am. Chem. Soc.*, 2008, **130**, 16721.
67 A. B. Robertson, A. Klungland, T. Rognes and I. Leiros, *Cell Mol. Life Sci*., 2009, **66**, 981.
68 P. J. O'Brien and T. Ellenberger, *Biochemistry*, 2003, **42**, 12418.
69 R. Rios-Font, L. Rodrguez-Santiago, J. Bertran and M. Sodupe, *J. Phys. Chem. B*, 2007, **111**, 6071.
70 Z. Chen, C. Zhang and Y. Xue, *J. Phys. Chem. B*, 2009, **113**, 10409.
71 A. L. Millen and S. D. Wetmore, *Can. J. Chem.*, 2009, **87**, 850.
72 R. Rios-Font, J. Bertran, M. Sodupe and L. Rodrguez-Santiago, *Theor. Chem. Acc.*, 2011, **128**, 619.
73 A. Ebriahimi, M. Habibi-Khorassani and S. Bazzi, *Phys. Chem. Chem. Phys.*, 2011, **13**, 3334.

74 A. C. Drohat and A. Maiti, *Org. Biomol. Chem.*, 2014, **12**, 8367.
75 J. Dong, A. C. Drohat, J. T. Stivers, K. W. Pankiewicz and P. R. Carey, *Biochemistry*, 2000, **39**, 13241.
76 S. Loverix, P. Geerlings, M. McNaughton, K. Augustyns, A. Vandemeulebroucke, J. Steyaert and W. Versees, *J. Biol. Chem.*, 2005, **280**, 14799.
77 J. A. B. McCann and P. J. Berti, *J. Am. Chem. Soc.*, 2008, **130**, 5789.
78 M. V. Rogacheva and S. A. Kuznetsova, *Russ. Chem. Rev.*, 2008, **77**, 765.
79 R. Wolfenden, *Annu. Rev. Biochem.*, 2011, **80**, 645.
80 M. Roger and R. Hotchkiss, *Proc. Natl. Acad. Sci. U.S.A.*, 1961, **47**, 653.
81 C. Tamm, H. S. Shapiro, R. Lipshitz and E. Chargaff, *J. Biol. Chem.*, 1953, **203**, 673.
82 R. R. Wu, B. Yang, G. Berden, J. Oomens and M. T. Rodgers, *J. Phys. Chem. B*, 2015, **119**, 2795.
83 R. R. Wu, B. Yang, C. E. Frieler, G. Berden, J. Oomens and M. T. Rodgers, *J. Phys. Chem B*, 2015, **119**, 5773.
84 R. R. Wu, B. Yang, C. E. Frieler, G. Berden, J. Oomens and M. T. Rodgers, *Phys. Chem. Chem. Phys.*, 2015, In press, DOI: 10.1039/c5cp02227d
85 R. R. Wu, B. Yang, C. E. Frieler, G. Berden, J. Oomens and M. T. Rodgers, *J. Am. Soc. Mass Spectrom.*, 2015, submitted.
86 C. Riml, H. Glasner, M. T. Rodgers, R. Micura and K. Breuker, *Nucleic Acids Res.* 2015, **43**, 5171.
87 M. T. Rodgers, *J. Phys. Chem. A*, 2001, **105**, 2374.
88 Y. Chen and M. T. Rodgers, *J. Am. Chem. Soc.*, 2012, **134**, 2313.
89 R. M. Moision and P. B. Armentrout, *J. Am. Soc. Mass Spectrom.*, 2007, **18**, 1124.
90 S. A. Shaffer, D. C. Prior, G. A. Anderson, H. R. Udseth and R. D. Smith, *Anal. Chem.*, 1998, **70**, 4111.
91 S. A. Shaffer, A. Tolmachev, D. C. Prior, G. A. Anderson, H. R. Udseth, and R. D. Smith, *Anal. Chem.*, 1999, **71**, 2957.
92 E. Teloy and D. Gerlich, *Chem. Phys.*, 1974, **4**, 417.
93 N. F. Dalleska, K. Honma and P. B. Armentrout, *J. Am. Chem. Soc.*, 1993, **115**, 12125.
94 N. Aristov and P. B. Armentrout, *J. Phys. Chem.*, 1986, **90**, 5135.
95 D. A. Hales and P. B. Armentrout, *J. Cluster Sci.*, 1990, **1**, 127.
96 N. R. Daly, *Rev. Sci. Instrum.*, 1960, **31**, 264.
97 K. M. Ervin and P. B. Armentrout, *J. Chem. Phys.*, 1985, **83**, 166.
98 N. F. Dalleska, K. Honma, L. S. Sunderlin and P. B. Armentrout, *J. Am. Chem. Soc.*, 1994, **116**, 3519.
99 M. J. Frisch, G. W. Trucks, H. B. Schlegel, G. E. Scuseria, M. A. Robb, J. R. Cheeseman, G. Scalmani, V. Barone, B. Mennucci, G. A. Petersson, H. Nakatsuji, M. Caricato, X. Li, H. P. Hratchian, A. F. Izmaylov, J. Bloino, G. Zheng, J. L. Sonnenberg, M. Hada, M. Ehara, K. Toyota, R. Fukuda, J. Hasegawa, M. Ishida, T. Nakajima, Y. Honda, O. Kitao, H. Nakai, T. Vreven, J. A. Montgomery, Jr., J. E. Peralta, F. Ogliaro, M. Bearpark, J. J. Heyd, E. Brothers, K. N. Kudin, V. N. Staroverov, R. Kobayashi, J. Normand, K. Raghavachari, A. Rendell, J. C. Burant, S. S. Iyengar, J. Tomasi, M. Cossi, N. Rega, J. M. Millam, M. Klene, J. E. Knox, J. B. Cross, V. Bakken, C. Adamo, J. Jaramillo, R. Gomperts, R. E. Stratmann, O. Yazyev, A. J. Austin, R. Cammi, C. Pomelli, J. W. Ochterski, R. L. Martin, K. Morokuma, V. G. Zakrzewski, G. A. Voth,

P. Salvador, J. J. Dannenberg, S. Dapprich, A. D. Daniels, Ö. Farkas, J. B. Foresman, J. V. Ortiz, J. Cioslowski, and D. J. Fox, Gaussian 09, Revision C.01; Gaussian, Inc.: Wallingford, CT, 2009.
100 C. Peng and H. B. Schlegel, *Israel J. of Chem.*, 1993, **33**, 449.
101 C. Peng, P. Y. Ayala, H. B. Schlegel and M. J. Frisch, *J. Comp. Chem.*, 1996, **17**, 49.
102 J. A. Jr. Montgomery, M. J. Frisch, J. W. Ochterski and G. A. Petersson, *J. Chem. Phys.*, 1999, **110**, 2822.
103 S. F. Boys and R. Bernardi, *Mol. Phys.*, 1970, **19**, 553.
104 F. B. van Duijneveldt, J. G. C. M. van Duijneveldt-van de Rijdt and J. H. van Lenthe, *Chem, Rev.*, 1994, **94**, 1873.
105 F. A. Khan, D. E. Clemmer, R. H. Schultz and P. B. Armentrout, *J. Phys. Chem.*, 1993, **97**, 7978.
106 M. T. Rodgers, K. M. Ervin and P. B. Armentrout, *J. Chem. Phys.*, 1997, **106**, 4499.
107 M. T. Rodgers and P. B. Armentrout, *J. Chem. Phys.*, 1998, **109**, 1787.
108 T. Beyer and D. F. Swinehart, *Commun. ACM*, 1973, **16**, 379.
109 S. E. Stein and B. S. Rabinovitch, *J. Chem. Phys.*, 1973, **58**, 2438.
110 S. E. Stein and B. S. Rabinovitch, *Chem. Phys. Lett.*, 1977, **49**, 183.
111 F. Muntean and P. B. Armentrout, *J. Chem. Phys*., 2001, **115**, 1213.
112 F. Muntean and P. B. Armentrout, *J. Phys. Chem. B*, 2002, **106**, 8117.
113 F. Muntean, L. Heumann and P. B. Armentrout, *J. Chem. Phys.*, 2002, **116**, 5593.
114 F. Muntean and P. B. Armentrout, *J. Phys. Chem. A*, 2003, **107**, 7413.
115 S. Narancic, A. Bach and P. Chen, *J. Phys. Chem. A*, 2007, **111**, 7006.
116 B. Jia, L. A. Angel and K. M. Ervin, *J. Phys. Chem. A*, 2008, **112**, 1773.
117 C. Ruan and M. T. Rodgers, *J. Am. Chem. Soc.*, 2009, **131**, 10918.
118 Y. Chen and M. T. Rodgers, *J. Am. Chem. Soc.*, 2012, **134**, 5863.
119 Y. Chen and M. T. Rodgers, *Anal. Chem.*, 2012, **84**, 7570.

Table 1. Relative Energies (kJ/mol) of the Reactants, Transition States, Intermediates and Products for Glycosidic Bond Cleavage Reactions of $[dGuo+H]^+$ and $[Guo+H]^+$.

CID Channel		Relative Energies[a]		CID Channel		Relative Energies[a]	
		B3LYP	MP2			B3LYP	MP2
$[Gua+H]^+$ from $[dGuo+H]^+$	TS_1	95.2	121.8	$[dGuo-Gua+H]^+$	TS_n	90.5	122.0
	Int_1	92.1	119.4		Int_n	86.6	120.5
	TS_2	94.3	132.7		ΔH_{rxn}	163.1	211.1
	Int_2	47.5	80.3		ΔH_{rxn} [b]	157.6	175.8
	ΔH_{rxn}	93.2	148.7				
	ΔH_{rxn} [b]	87.0	102.9				
$[Gua+H]^+$from $[Guo+H]^+$	TS_1	117.8	149.4	$[Guo-Gua+H]^+$	TS_n	84.5	109.0
	Int_1	49.1	33.9		Int_n	76.3	108.0
	TS_2	120.9	157.0		ΔH_{rxn}	184.7	237.3
	Int_2	28.3	64.0		ΔH_{rxn} [b]	178.8	200.2
	ΔH_{rxn}	93.7	157.0				
	ΔH_{rxn} [b]	86.8	107.9				

[a]B3LYP/6-311+G(2d,2p) and MP2/6-311+G(2d,2p) relative energies of B3LYP/6-311+G(d,p) optimized structures at 0 K including ZPE corrections with frequencies scaled by 0.99.
[b]BSSE corrections are included for the final reaction products.

Table 2. Fitting Parameters of Equation 2, Threshold Energies at 0 K and Entropies of Activation at 1000 K of $[dGuo+H]^+$ and $[Guo+H]^+$.[a]

Reactant	CID Products	σ_0 [b]	n [b]	E_0 [b] (eV)	$\Delta S^{\ddagger}$ (J/mol·K)
$[dGuo+H]^+$[c]	$[Gua+H]^+$	79.1 (4.2)	2.1 (0.1)	0.97 (0.03)	25 (1)
	$[dGuo-Gua+H]^+$	1.3 (0.2)	2.1 (0.1)	1.72 (0.04)	99 (4)
$[Guo+H]^+$[c]	$[Gua+H]^+$	73.4 (3.0)	2.1 (0.1)	1.19 (0.03)	38 (1)
	$[Guo-Gua+H]^+$	0.9 (0.1)	2.1 (0.1)	2.01 (0.06)	101 (4)

[a]Present results, uncertainties are listed in parentheses. [b]Average values from threshold analysis. [c]Values obtained from competitive analyses using TTS + switching TS models for lifetime modeling.

Table 3. Activation Energies and Reaction Enthalpies for N-Glycosidic Bond Cleavage of $[dGuo+H]^+$ and $[Guo+H]^+$ at 0 K in kJ/mol.[a]

Ionic Product	TCID[b]		B3LYP[c]			MP2[d]		
	AE	ΔH_{rxn}	AE	ΔH_{rxn}	ΔH_{rxn}[e]	AE	ΔH_{rxn}	ΔH_{rxn}[e]
$[Gua+H]^+$ from $[dGuo+H]^+$	93.6 (2.9)	-	95.2	93.2	87.0	132.7	148.7	102.9
$[dGuo-Gua+H]^+$	-	166.0 (3.9)	90.5	163.1	157.6	122.0	211.1	175.8
$[Gua+H]^+$ from $[Guo+H]^+$	114.8 (2.9)	-	120.9	93.7	86.8	157.0	157.0	107.9
$[Guo-Gua+H]^+$	-	193.9 (5.8)	84.5	184.7	178.8	109.0	237.3	200.2
AEU[f]	2.9 (0.0)	4.9 (1.3)						
MAD[g]			3.9 (3.2)	6.1 (4.5)	11.8 (4.7)	40.7 (2.2)	44.3 (1.2)	8.1 (2.5)

[a]Present results, uncertainties are listed in parenthess. [b]TCID activation energies and reaction enthalpies obtained from competitive threshold analyses. [c]Calculated at B3LYP/6-311+G(2d,2p)//B3LYP/6-311+G(d,p) level of theory including ZPE corrections. [d]Calculated at MP2(full)/6-311+G(2d,2p)//MP2(full)/6-311+G(d,p) level of theory including ZPE corrections. [e]Also includes BSSE corrections. [f]Average experimental uncertainty (AEU). [g]The mean absolute deviation (MAD) between calculated and experimentally obtained AEs and ΔH_{rxn}.

Table 4. Relative Energies (kJ/mol) of the Reactants, Transition States, Intermediates and Products for Producing $[Gua+H]^+$ from $[dGuo+H]^+$ and $[Guo+H]^+$ With Polarizable Continuum Model.

CID Channel		Relative Energies[a]		CID Channel		Relative Energies[a]	
		B3LYP	MP2			B3LYP	MP2
$[Gua+H]^+$ from $[dGuo+H]^+$	TS_1	91.1	117.0	$[Gua+H]^+$ from $[Guo+H]^+$	TS_1	112.1	142.9
	Int_1	88.7	116.5		Int_1	47.4	31.8
	TS_2	94.2	132.7		TS_2	124.3	160.4
	Int_2	37.0	69.2		Int_2	26.8	62.1
	ΔH_{rxn}	42.8	97.5		ΔH_{rxn}	43.2	105.7
	ΔH_{rxn}[b]	36.6	51.7		ΔH_{rxn}[b]	36.2	56.7

[a]B3LYP/6-311+G(2d,2p) and MP2/6-311+G(2d,2p) relative energies of B3LYP/6-311+G(d,p) optimized structures at 0 K including ZPE corrections with frequencies scaled by 0.99.
[b]BSSE corrections are included for the final reaction products.

Figure Captions

Figure 1. Chemical structures of neutral 2'-deoxyguanosine (dGuo) and guanosine (Guo) and B3LYP/6-311+G(d,p) ground-state structures of $[dGuo+H]^+$ and $[Guo+H]^+$. The preferred site of protonation, nucleobase orientation, and sugar puckering are indicated for each protonated nucleoside.

Figure 2. Cross sections for collision-induced dissociation of $[dGuo+H]^+$ and $[Guo+H]^+$ with Xe as a function of kinetic energy in the center-of-mass frame (lower *x*-axis) and laboratory frame (upper *x*-axis), parts a and b, respectively. The CID pathways for glycosidic bond cleavage leading to the production of protonated guanine, $[Gua+H]^+$, and to the elimination of neutral guanine, Gua are shown as solid blue circles and red triangles, respectively. Products arising from sequential dissociation of the charged sugar moieties, $[dGuo-Gua+H]^+$ and $[Guo-Gua+H]^+$, are shown as small open red symbols. See Table S3 for the identities of these sequential fragments. Data are shown for a Xe pressure of 0.2 mTorr.

Figure 3. Calculated potential energy surfaces for the production of $[Gua+H]^+$ and $[dGuo-Gua+H]^+$ from $[dGuo+H]^+$, parts a and b, respectively. Structures were optimized at the B3LYP/6-311+G(d,p) level of theory, whereas energetics are shown based on B3LYP/6-311+G(2d,2p) (shown in blue) and the MP2(full)/6-311+G(2d,2p) (shown in red) single point energies and include zero-point energy corrections for all species, and BSSE corrections for the dissociation products.

Figure 4. Calculated potential energy surfaces for the production of $[Gua+H]^+$ and $[Guo-Gua+H]^+$ from $[Guo+H]^+$, parts a and b, respectively. Structures were optimized at the B3LYP/6-311+G(d,p) level of theory, whereas energetics are shown based on B3LYP/6-

311+G(2d,2p) (shown in blue) and the MP2(full)/6-311+G(2d,2p) (shown in red) single point energies and include zero-point energy corrections for all species, and BSSE corrections for the dissociation products.

Figure 5. Zero-pressure-extrapolated $[Gua+H]^+$ and $[Nuo-Gua+H]^+$ CID product cross sections of $[dGuo+H]^+$ and $[Guo+H]^+$, where Nuo = dGuo and Guo, in the threshold region, parts a and b, respectively. The solid lines show the best fits to the data using eq 2 convoluted over the ion and neutral kinetic energy distributions. The dotted lines show the model cross sections in the absence of experimental kinetic energy broadening for reactants with an internal energy corresponding to 0 K.

Figure 6. Comparison of theoretical 0 K AEs and ΔH_{rxn}s for N-glycosidic bond cleavage of $[dGuo+H]^+$ and $[Guo+H]^+$ vs the corresponding TCID measured threshold energies. All values are taken from Table 3.

Figure 1.

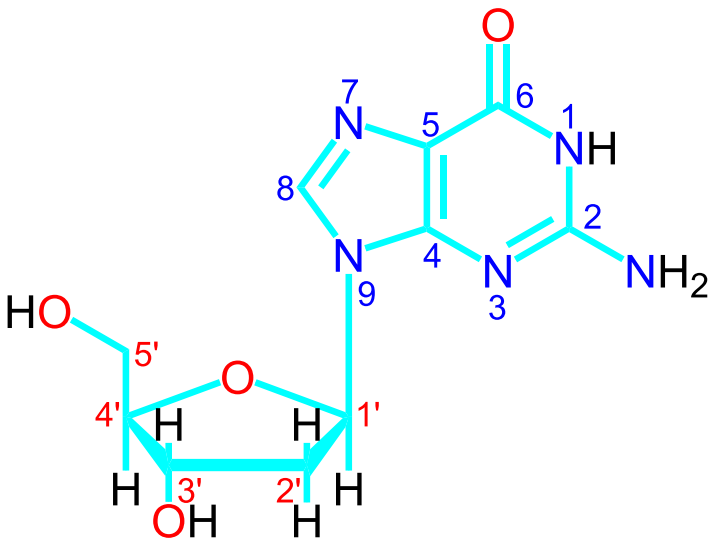

dGuo
2'-Deoxyguanosine

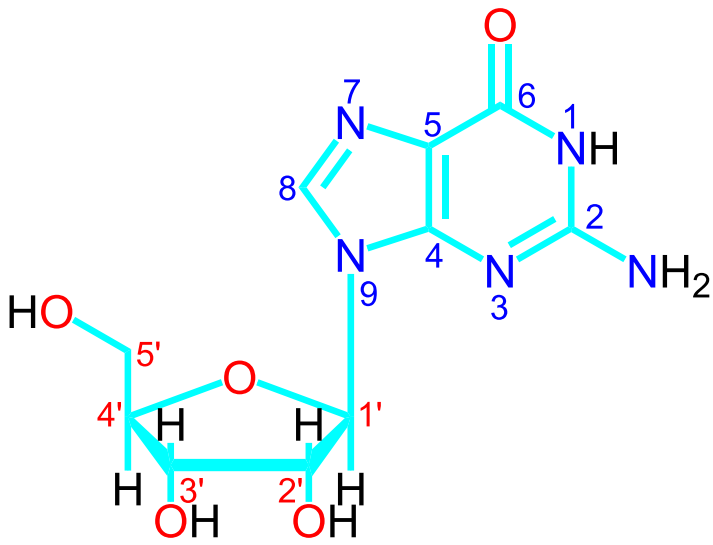

Guo
Guanosine

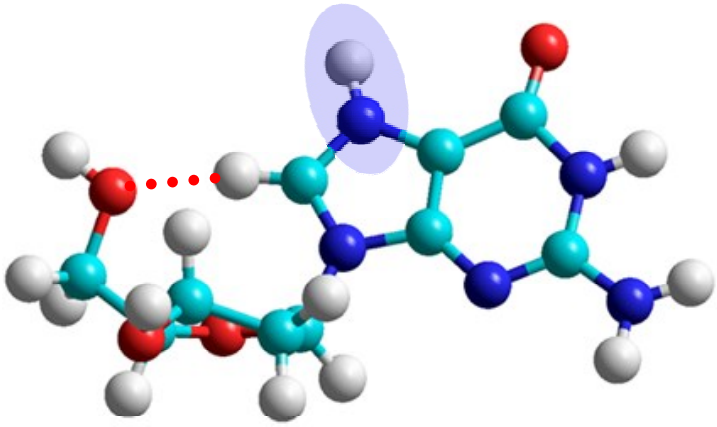

[dGuo+H]+
N7, anti, C3'-endo

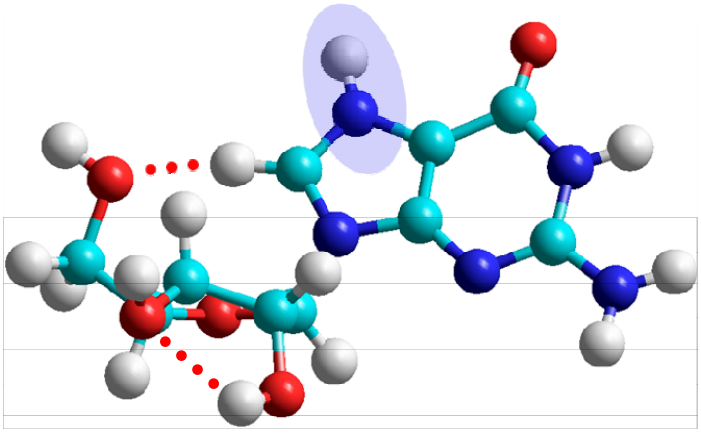

[Guo+H]+
N7, anti, C3'-endo

Figure 2.

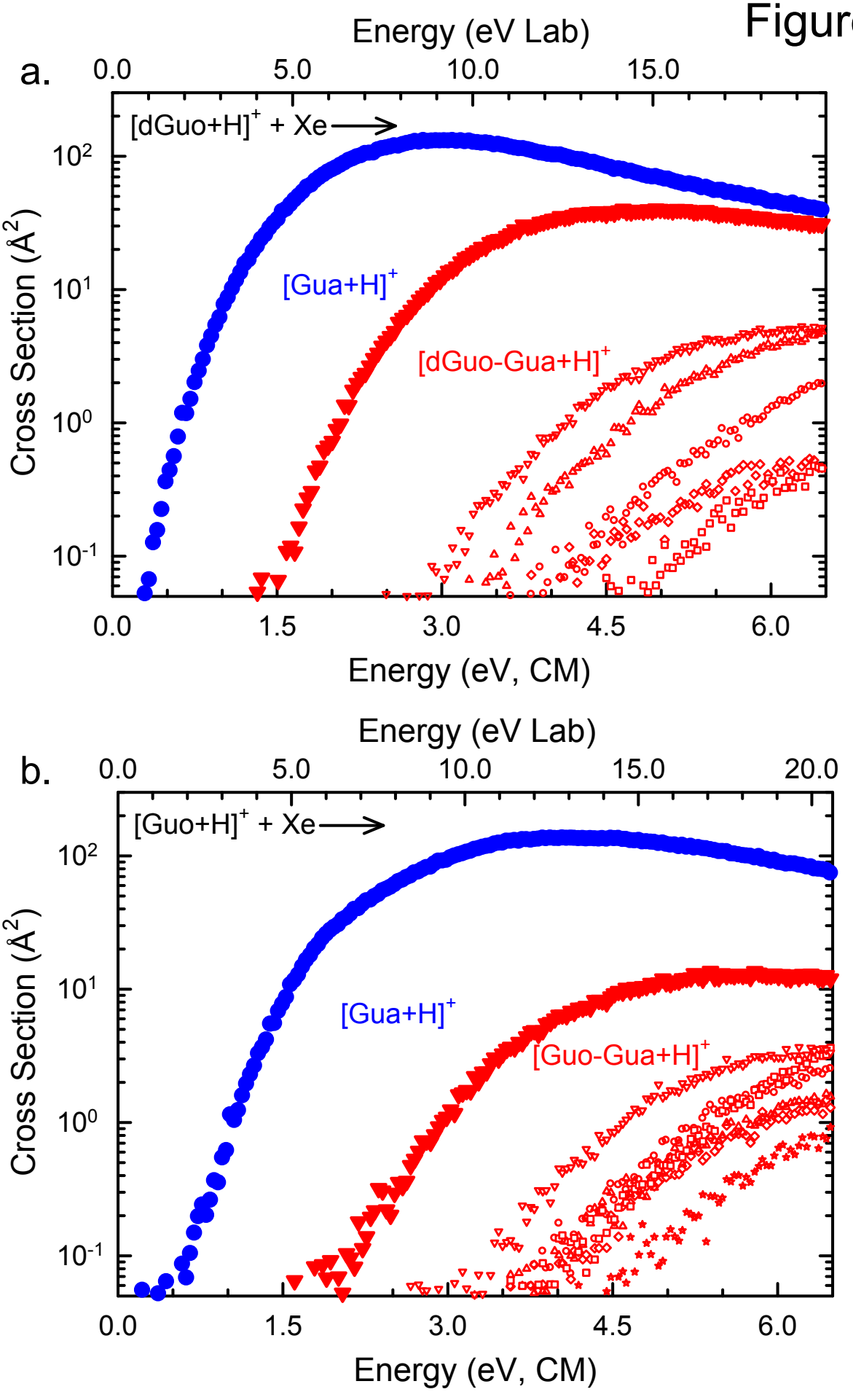

Figure 3.

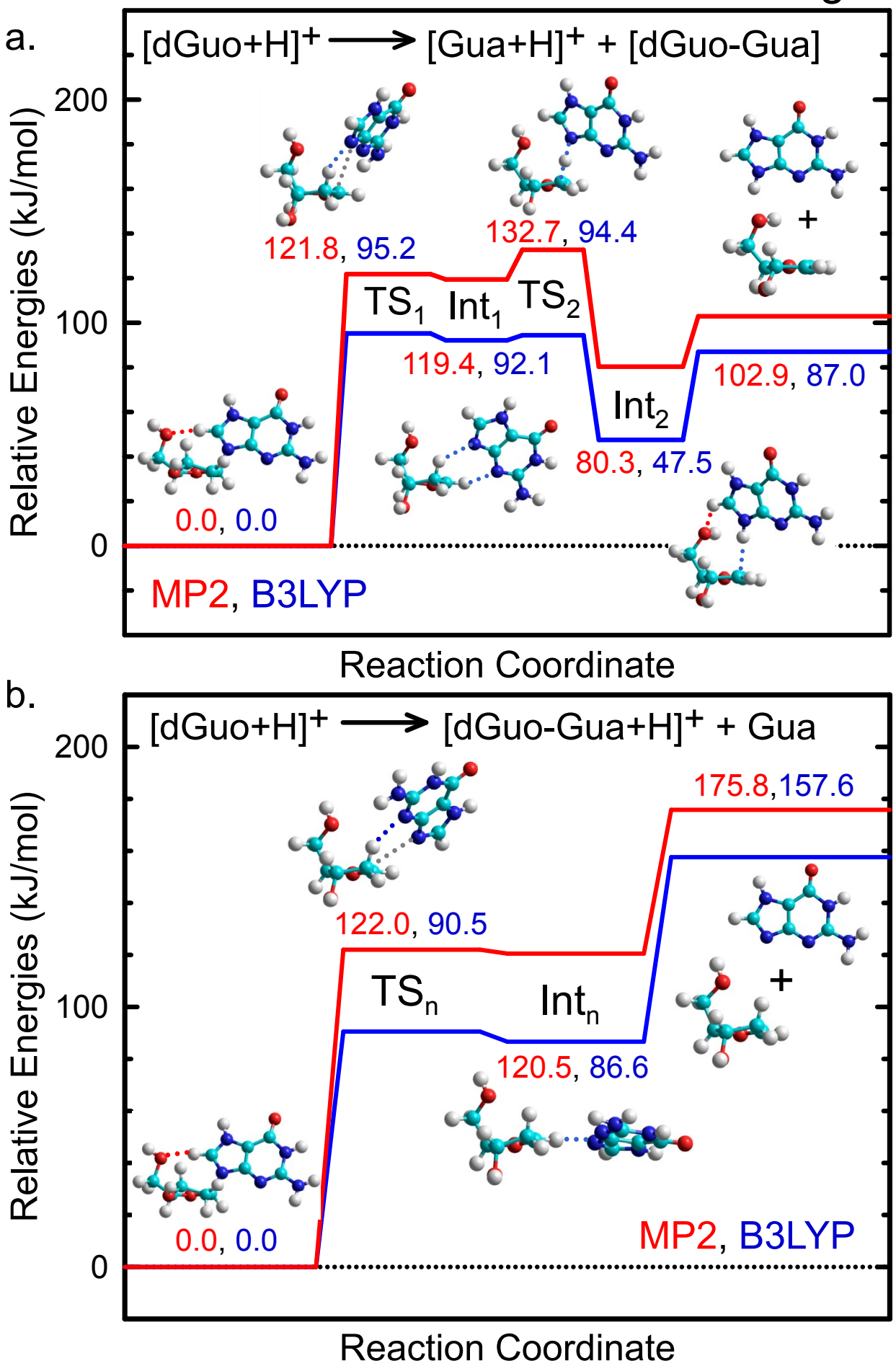

Figure 4.

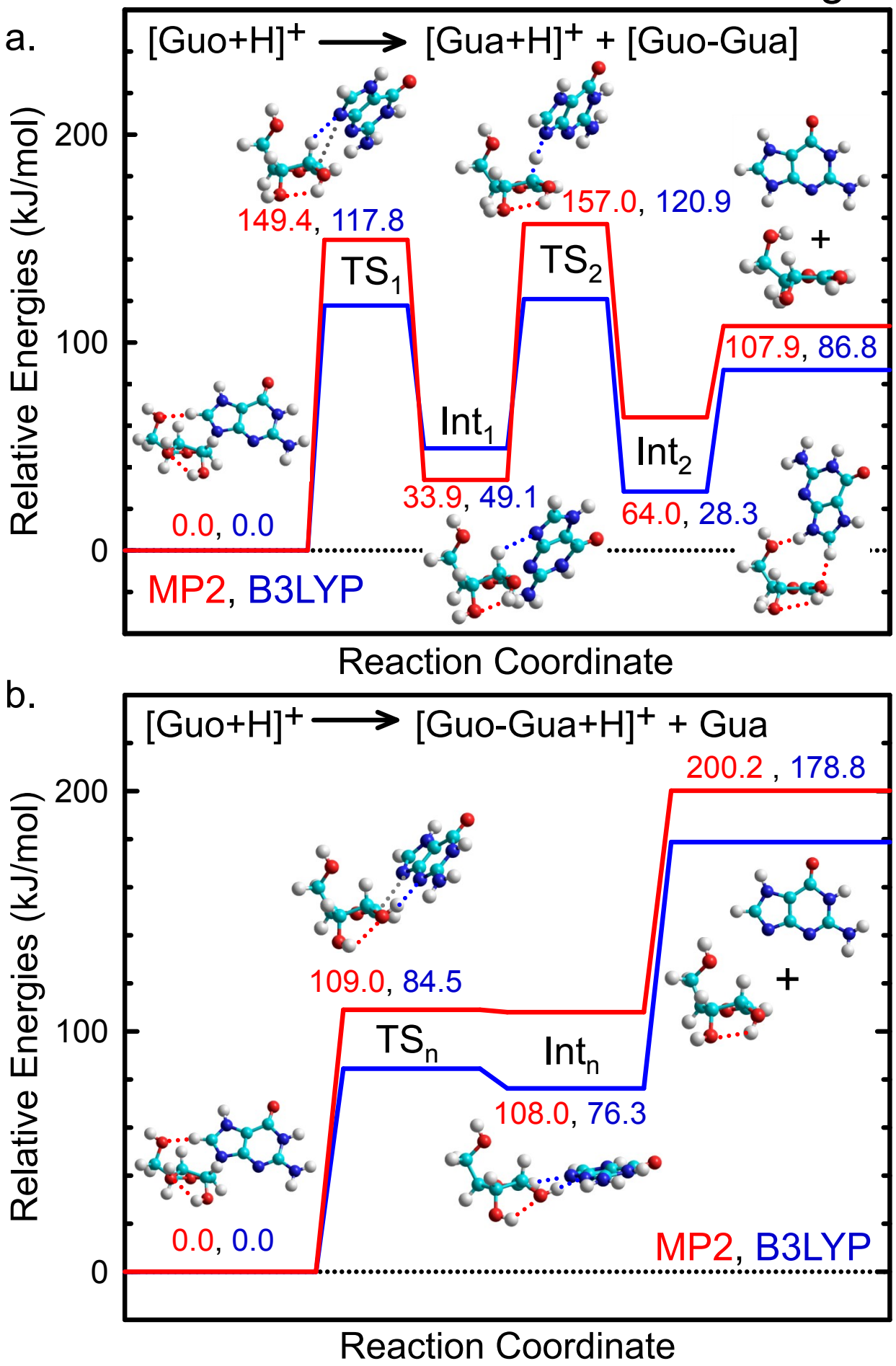

Figure 5.

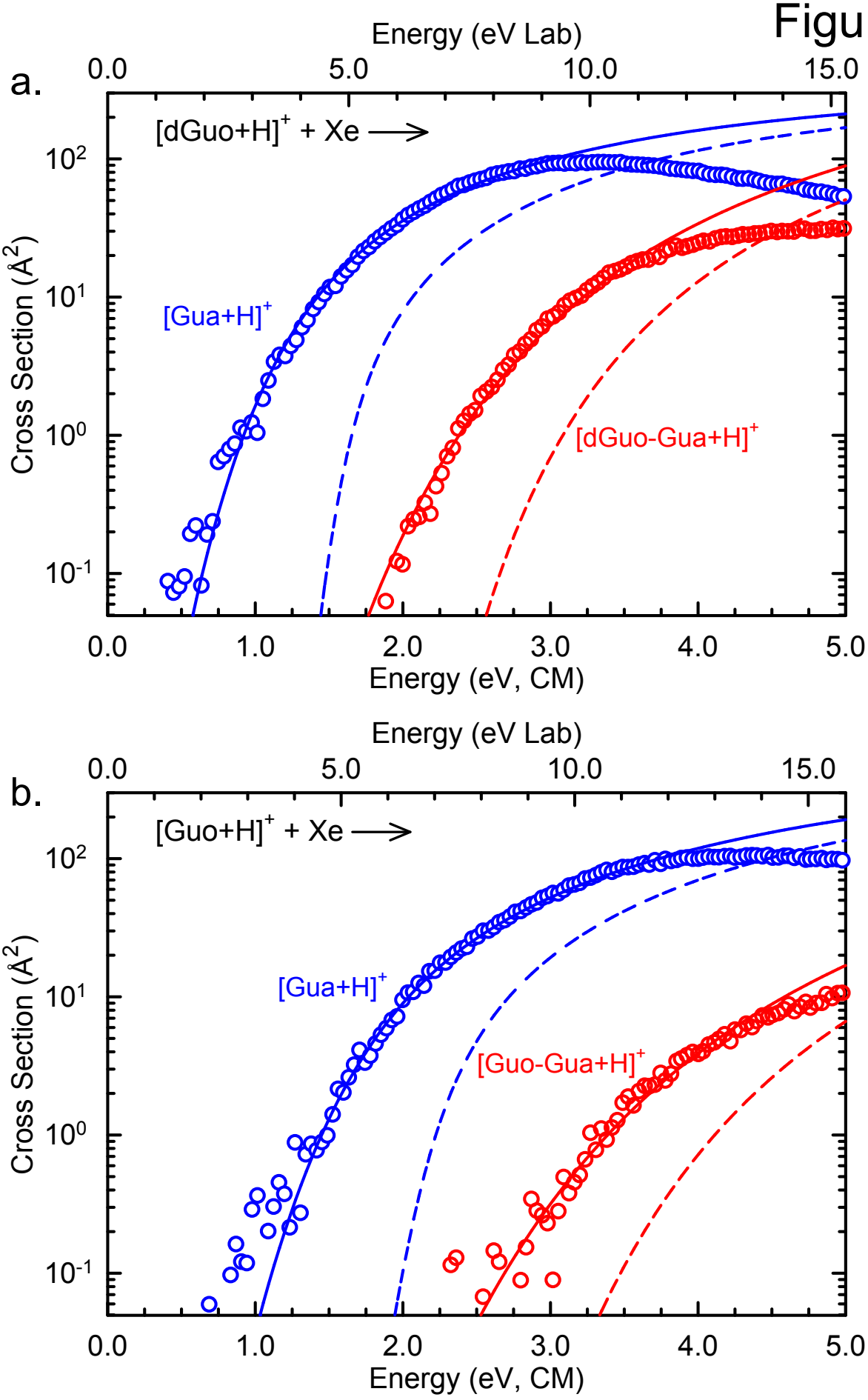

Figure 6.